Cold Regions Science and Technology 154 (2018) 32–41

Contents lists available at ScienceDirect

Cold Regions Science and Technology

journal homepage: www.elsevier.com/locate/coldregions

Monitoring snowbank processes and cornice fall avalanches with time-lapse photography

Jeffrey S. Munroe*

Geology Department, Middlebury College, Middlebury, VT 05753, United States

ARTICLE INFO

Keywords:
Snowbank
Cornice
Avalanche
Time-lapse photography

ABSTRACT

Time-lapse photography was employed to monitor a snowbank at 3640 m above sea level in the Uinta Mountains, Utah, USA. The snowbank forms against a 35-m high, east-facing escarpment and is nourished by wind redistribution of snow from an alpine plateau. The snowbank is capped by a large cornice, and its central core persists through the summer in most years. An automated, solar-powered digital camera was deployed between October 2016 and June 2017, and programmed to capture 5 photographs each day between 8:00 and 16:00, local time. Although cold temperatures affected the batteries during the winter, a total of 812 photographs were collected, for an overall average of 3.4 per day. These images were combined in an animation displaying the growth of the snowbank and associated cornice over the course of the winter. The debris fields resulting from nineteen cornice fall avalanches were noted in the sequence of photographs. Data collected at a nearby automated weather station reveal that 12 avalanches (between early December and early April) were preceded by significant increases in snow depth, snow water equivalent, and precipitation, with sustained windspeeds above the winter average. In contrast, six of the last seven events (between late April and early June) occurred in the absence of new snowfall, but were associated with rapid rises in temperature and notable decreases in snow water equivalent. The average interval between recorded avalanches is 10 days, with a maximum of 29 days and a minimum of 2 h. Recurrence intervals were shorter in December/January, in late March/early April, and in late April/early May. Only one avalanche occurred in the 56 days between 27 January and 24 March. Time-lapse photography is a powerful tool for monitoring nival processes.

1. Introduction

Many natural processes operate on timescales that preclude direct visual observation. This problem is enhanced for events that are inherently difficult to predict. In the context of cryosphere research, numerous processes associated with the accumulation and melting of snow are challenging to observe directly and to monitor continuously. These include the episodic growth of snowbank cornices (Kobayashi et al., 1988; McCarty et al., 1986), avalanching related to cornice collapse (Eckerstorfer and Christiansen, 2011), and the proposed enhancement of erosion in areas surrounding snowbanks referred to by the collective term “nivation” (Dohrenwend, 1984; Matthes, 1900; Thorn, 1988).

Repeat photography is commonly employed to document landscape change (Klett, 2004, 1984; Klett et al., 2011; Webb, 1996). Time-lapse photography is an enhanced version of repeat photography, where multiple photographs are collected at specific intervals from a common vantage point (Malin, 2007). With a camera mounted in a fixed location, sequences of time-lapse photographs can be combined to create an animation illustrating landscape change (Campbell and Egbert, 1990). Advances in digital camera technology, combined with the ready availability of solar powered charging systems, have made it possible to automatically collect sequences of photographs in remote locations over periods of months to years. Perhaps the most familiar utilization of this technology is the striking animations of glacier change collected by the Extreme Ice Survey and presented in the movie “Chasing Ice” (Balog, 2012; Burkhart et al., 2017).

Recently, studies have begun to apply time-lapse techniques to the monitoring of snowbanks, cornices, and avalanching (Eckerstorfer et al., 2016, 2013b, 2013a; van Herwijnen et al., 2013; van Herwijnen and Fierz, 2014; Vogel et al., 2012). Much of this work (e.g. Eckerstorfer et al., 2013b, 2013a; Vogel et al., 2012), however, was conducted in the High Arctic under conditions of relatively minor snowfall, extensive permafrost, sustained cold temperatures, and lack of mid-winter solar radiation. Thus, it is unclear how broadly applicable these results are to settings at lower latitudes. Furthermore, most

* Corresponding author.
E-mail address: jmunroe@middlebury.edu.

https://doi.org/10.1016/j.coldregions.2018.06.006
Received 17 January 2018; Received in revised form 5 June 2018; Accepted 12 June 2018

studies that have used time-lapse photography in lower latitude mountains (e.g. Dreier et al., 2016; Hendrikx et al., 2012; van Herwijnen and Simenhois, 2012) focused on glide avalanches, which are distinct from cornice fall events in terms of their triggers and movement style. One exception is a study in Switzerland that used time-lapse photography to document cornice growth (van Herwijnen et al., 2013). However, the onset of cornice growth was not captured in this project because the camera was installed after snow accumulation had begun, and no cornice collapse events occurred during the winter.

Because the incorporation of time-lapse photography in avalanche studies is still in its infancy, and this technique has not been extensively applied to cornice fall avalanches in mid-latitude mountains, this project pursued two parallel objectives. First, the utility of time-lapse photography as a tool for monitoring nival processes in a continental mountain setting with a relatively warm, deep snowpack was explored. The automated camera was deployed for eight months and multiple episodes of cornice construction and avalanching where recorded. The second objective was to compare the timing of these avalanches with meteorological data to identify controls on cornice collapse in this setting.

2. Methods

2.1. Study site

The study site for this project is in the Uinta Mountains of northeastern Utah, USA (Fig. 1A). At this location, a ~400-m wide expanse of treeless, alpine tundra ends abruptly at a 35-m high east-facing escarpment (Fig. 1A). Large amounts of snow are transported from this tundra surface by the wind each winter, forming a large snowbank against this escarpment at an elevation of ~3640 m above sea level. The central core of this snowbank persists throughout the summer in most years (Fig. 1B), resembling snowpatches called "firns" in a previous study (Wahl et al., 2009). At the top of the snowbank, an extensive cornice forms along the plateau edge (Fig. 1C and D). Cornices are distinctive, cantilevered snowbanks (Fig. 1D) produced by wind redistribution of snow (McCarty et al., 1986). They often exhibit a relatively flat "roof" that projects outward above a vertical scarp. The leading edge of this roof curls downward forming a steep cornice face, and may overhang to produce a partially enclosed "roll cavity" (Montagne et al., 1968; Vogel et al., 2012). Tension cracking along the backside of the roof can lead to detachment and cornice fall, depending on microtopography (Vogel et al., 2012). Cornices are common features in mountain environments and are not rare in the Uinta Mountains. This particular site was selected because observations over multiple years illuminate the typical growth and ablation pattern of the cornice and associated snowbank. This remote location also reduced the possibility that the camera would be disturbed.

Meteorological conditions during the camera deployment were constrained by data from three different sources. First, hourly and daily data for air temperature, precipitation, and snowfall at the Steel Creek Park snowpack telemetry (SNOTEL) site, approximately 500 m lower and 10 km to the north, were downloaded from the Natural Resource Conservation Service < https://wcc.sc.egov.usda.gov/nwcc/site?sitenum=790 >. This site has a mean annual air temperature of 1.4 °C and receives ~760 mm of precipitation each year. Snow accumulates here to an average April depth of ~125 cm and exhibits features of an alpine snowpack (Sturm et al., 1995). Second, daily values for temperature and precipitation for the snowbank site during the period of the camera deployment were obtained from the interpolated dataset produced by the PRISM Climate Group < http://prism.oregonstate.edu/explorer >. These values exhibit strong linear correspondence with data from the SNOTEL site (daily precipitation $r^2 = 0.842$; daily minimum temperature $r^2 = 0.971$; daily maximum temperature $r^2 = 0.984$), and reveal that the higher elevation snowbank site has a mean annual temperature of ~ −1.8 °C and receives ~950 mm of precipitation annually. Finally, measurements of wind speed and direction were collected at the Chepeta Remote Automated

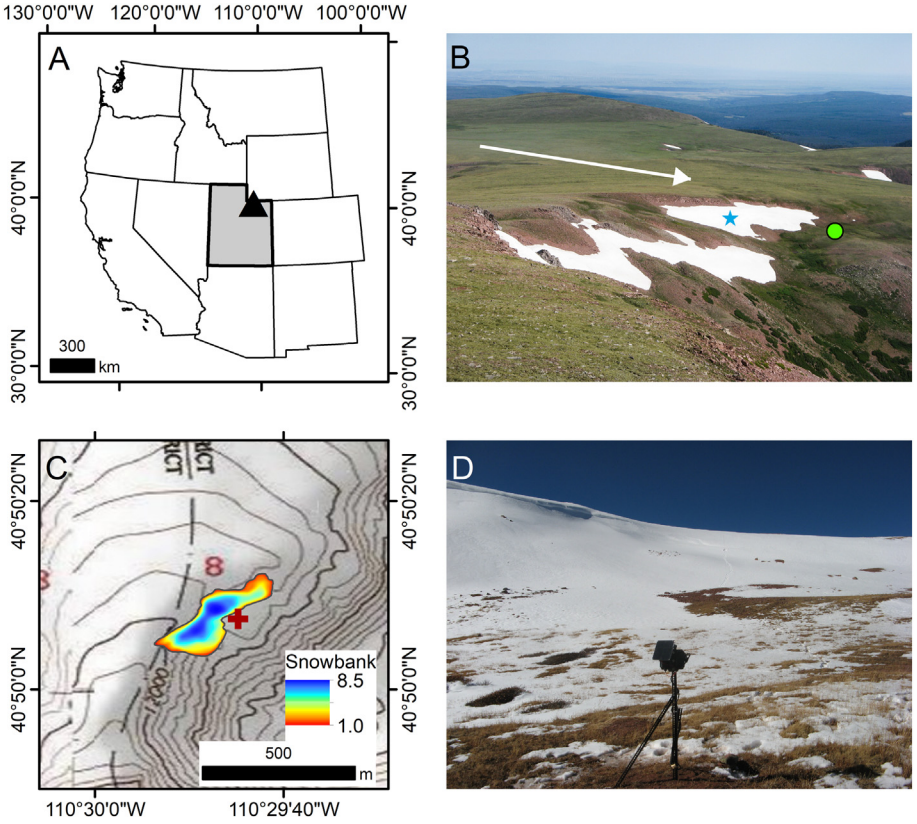

Fig. 1. (A) Oblique photograph (23 July 2014) northward across the study area. Green dot marks the camera location and blue star identifies the studied snowbank. The arrow denotes the prevailing wind direction. Note the expanse of treeless tundra to the west of the snowbank. Inset shows the location of the study area (star) in northeastern Utah. (B) Position of the snowbank displayed over a topographic map with 40-ft contour intervals. The dark red cross represents the camera location. The color shading is a heatmap compiled from vertical aerial imagery of the snowbank over 9 separate summers; shading represents the number of photographs in which that part of the snowbank was present. Sectors of the snowbank, therefore, inferred to be thinner are shown in redder colors; inferred thicker snow is shown in blue. (C) Picture of the installed camera aimed at the snowbank on 21 October 2016. The shadowed face of the cornice is visible at the top of the snowbank. (D) Sketch illustrating the arrangement of the camera and measuring pole relative to the cornice and snowbank.

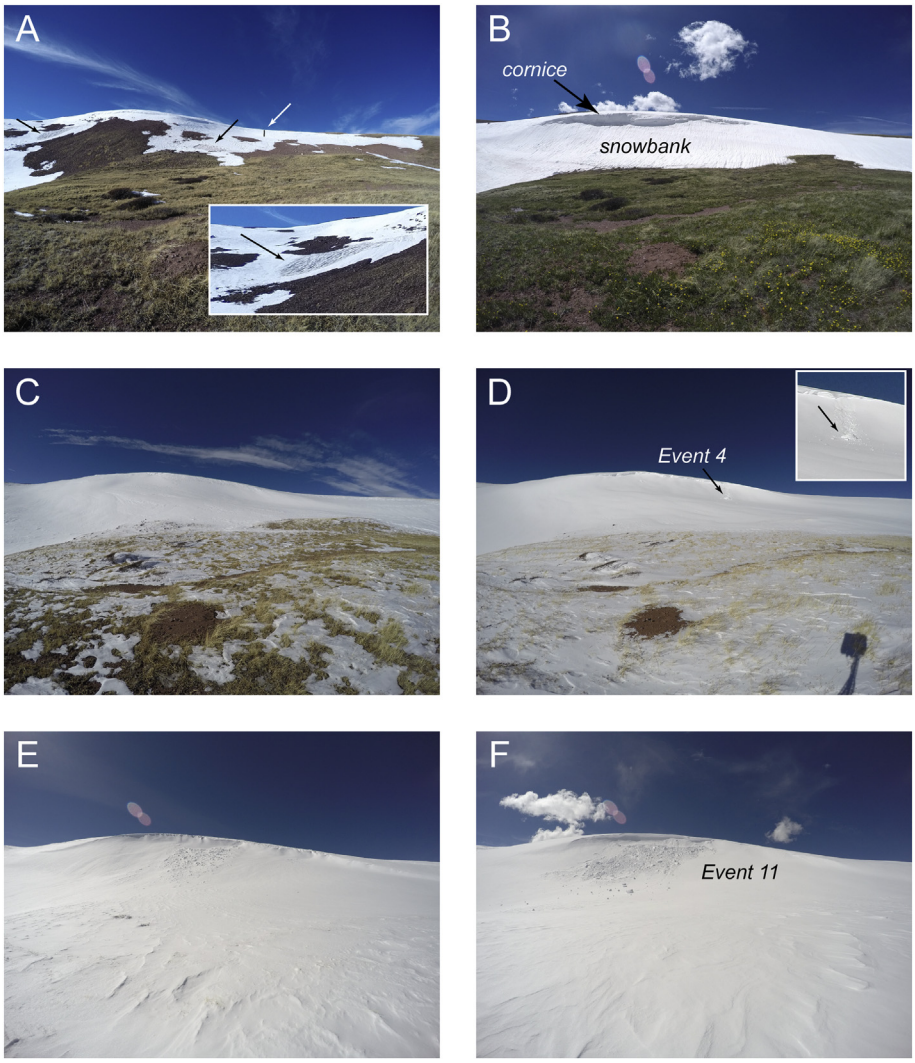

Fig. 2. Example photographs of the snowbank during deployment of the camera. The field of view is roughly 150 m wide at the horizon. (A) Photograph of the snowbank at its minimum extent on 14 November 2016, prior to the first snowstorm of the season. The white arrow marks the 3-m tall pole (highlighted in black) used to measure snow depth and estimate height of the cornice (see Fig. 1D). The two black arrows denote the patches of old firn that emerged from the snowbank in the last few weeks of ablation. The inset presents an enlargement of the firn patch in the upper left corner of the main image. (B) Photograph of the snowbank and cornice near the end of the camera deployment on 16 June 2017. (C & D) Photographs bracketing Event 4, a relatively small cornice collapse in early January. The inset in panel D presents an enlargement of the collapsed cornice section. (E & F) Photographs bracketing Event 11, a larger debris field produced by cornice collapse in early April. (For interpretation of the references to color in this figure legend, the reader is referred to the web version of this article.)

Weather Station (RAWS) ~35 km to the east < https://raws.dri.edu/cgi-bin/rawMAIN.pl?utCHEP >. Despite the distance separating the Chepeta RAWS from the snowbank site, use of data from Chepeta is justified because both sites are at the same elevation, both are located above treeline, and both offer similar exposure to prevailing winds.

2.2. Photography

A GoPro Hero 4 Silver digital camera was deployed at an elevation of 3620 m above sea level, aimed to the west, facing directly at the snowbank (Fig. 1C and D). A 1.5-m long metal post was pounded into the ground with a sledgehammer, and a weathertight case for the camera was attached to this post using tamperproof screws. The post was braced with additional metal rods, forming a stable tripod. A 6-W solar panel mounted on top of the post powered a 15-Wh battery inside the camera case. The camera lens was covered with a 67-mm ultraviolet filter. To serve as a vertical scale, a 3.8-m long pole of 2.5-cm-diameter, white pvc pipe graduated at 50-cm intervals with wraps of colored tape was installed in the central sector of the snowbank (Figs. 1D and 2A). Three meters of the pipe extended above the snow surface at the time of deployment.

The camera was configured to collect 12-megapixel images in a 4 × 3 format using a lens with a 17.2-mm focal length and f/2.8. The timer was programmed to take five pictures each day, at a 2-h interval starting at 8:00 Mountain Standard Time (UTC - 7:00). The camera was deployed on 21 October 2016 and retrieved on 18 June 2017 (240 days).

2.3. Data analysis

Images captured by the camera as .jpg files were combined to create an animation showing the evolution of the snowbank during the period of deployment. Individual photographs recording the debris fields from new snow avalanches were identified, and their time and date were noted. In addition, the most recent preceding photograph with a clear view lacking avalanche evidence was identified to constrain when each event occurred. The exact timing of an avalanche within this interval cannot be determined, but for brevity and consistency the time between each pair of photographs is referred to hereafter as the “pre-avalanche interval.”

Photographs documenting each avalanche were appended with identical, arbitrary world files and imported to ArcGIS 10.3 where the debris field produced by each avalanche was traced to produce a polygon shapefile. Shapefiles were converted to rasters, which were summed using raster algebra to generate a heatmap (Wilkinson and Friendly, 2009) displaying the frequency of avalanches across the face of the snowbank. The width of the cornice sector involved in each avalanche (as a proxy for avalanche magnitude), and the height of the vertical cornice face, were measured in pixels. Cornice face measurements were made at a common point on each photograph, and were converted to meters given the pixels/m ratio of the measuring pole visible in the early photographs (Figs. 1D and 2A).

Using the available meteorological data, the amount of precipitation and snow accumulation, the magnitude of temperature change, and the mean temperature, wind speed, and wind direction (as a circular mean) during each pre-avalanche interval were determined. Rates of changes in precipitation, snow depth, and temperature were calculated over 5-h periods throughout each pre-avalanche interval, and the maximum positive and negative rates in each interval were recorded. A 5-h step was selected as a compromise between shorter intervals that failed to represent the typical durations of storm events, and longer intervals that smoothed too much variability in precipitation and temperature. On the basis of these data, avalanches were assigned to groups with contrasting triggers: snow-caused and temperature-caused.

Values constraining the timing and dimensions of each avalanche, along with meteorological data for each pre-avalanche interval, were imported to SPSS 24.0 for statistical analysis. Differences between the snowfall and temperature groups were assessed with a Mann-Whitney test. A nonparametric test was employed because of the relatively small number of observations and the unequal number of observations in each group. Multiple linear regression was implemented using automatic linear modeling to identify variables most closely associated with failed cornice width. A forward stepwise model was employed with the adjusted r^2 value as a criterion for inclusion in the model. This analysis was conducted initially for the entire avalanche dataset, and was repeated for the subsets of snow and temperature-caused events.

Finally, georectified vertical aerial images displaying the snowbank on different summer days in 9 years between 1993 and 2017 were accessed in Google Earth. The outline of the snowbank on each of these images was digitized, imported to ArcGIS, and converted to a raster. These were then summed with raster algebra to produce a heatmap revealing the pattern through which the snowbank annually ablates. Although the thickness of the snowbank was not directly measured, this map likely reflects a qualitative estimate of snow depth, assuming that the thinner parts of the snowbank melt first each year.

3. Results

3.1. Photographs

When accessed on 18 June 2017, the camera was still functioning and exhibited no signs of disturbance. The memory card held 812 photographs (average of 3.4/day), which is 67% of the 1200 expected over 240 days. Consideration of the time stamps on the image files reveals that a full complement of 5 photographs was taken on 90 days (38%), and 3 or 4 photographs were taken on 80 days. No photographs were taken on 21 days (9%); 16 of these were in a continuous stretch in early May when the camera unexpectedly turned off. Furthermore, due to an unexplained error in the camera controller, the times at which photographs were taken shifted to later in the day starting in late February. As a result, some photographs were taken at night. Removing these yields a set of 699 useable images, for an average of 2.9 per day.

Early photographs (Fig. 2A) document diminishment of the snowbank toward its annual minimum extent. The surface of the snowbank lowered slowly through a combination of settling and ablation (Fig. 3). The first major snowstorm occurred on 17 November, delivering 20 cm of snow to the SNOTEL site. Hourly average windspeeds at Chepeta during this storm exceeded 17 m/s and the depth of snow at the measuring pole in the snowbank increased by 1.0 m (Fig. 3). A second storm on 22 November brought 12.5 cm of snow to the SNOTEL site with mean hourly wind speeds in excess of 20 m/s, increasing the snow depth at the pole to 1.7 m (Fig. 3). A third snowstorm between the 26 and 29, November deposited 33 cm of snow at the SNOTEL site. Hourly average windspeeds peaked at 18 m/s, and were sustained at velocities > 13 m/s for 15 h. After this storm, the measuring pole was no longer visible, indicating a new snow accumulation of > 2.0 m and a snow depth in excess of 3.8 m (Fig. 3). No bare ground or vegetation was visible between 25 March and 3 May 2017, but melting proceeded rapidly in May. The tundra at the foot of the snowbank was fully exposed after 1 June, although the snowbank and associated cornice were still extensive when the camera deployment ended on 18 June (Fig. 2B).

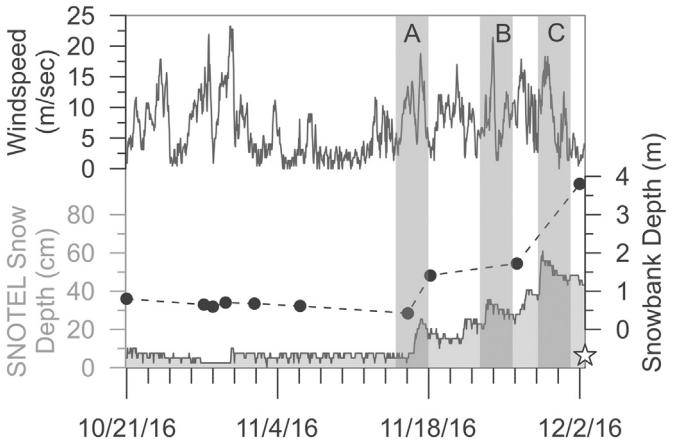

Fig. 3. Snow depth at the snowpack telemetry (SNOTEL) station (filled gray line) compared with snow depth at the measuring pole in the snowbank (dashed black line with circles) and mean hourly windspeed at the Chepeta weather station (top). Slow lowering of the snowbank surface occurred over the first few weeks of the camera deployment. The 3.8-m tall pole (Figs. 1D & 2A) disappeared from view following three separate storms (A, B, C) in late November that delivered notable snow accumulations accompanied by strong winds.

3.2. Avalanches

Nineteen avalanches were noted between 2 December 2016 and 2 June 2017 (Fig. 4). Three occurred in December, 4 in January, 1 in February, 2 in March, 4 in April, 4 in May, and 1 in June (Table 1). The average duration of the pre-avalanche interval determined from the photographs bracketing each avalanche is 2.5 days (Table 1). This average decreases to 1.7 days when the 16-day period in which the camera was dormant is removed. Given the temporal gaps between the photographs it is not possible to determine whether an avalanche debris field represents a single event, or a composite of multiple failures closely spaced in time. For simplicity, each photograph displaying newly avalanched material is assumed to represent a single collapse.

All but the last of the 19 events were cornice fall avalanches (Eckerstorfer and Christiansen, 2011). In some avalanches, only a single part of the cornice fell (Fig. 2 C&D), whereas in other events wide sections of the cornice collapsed (Fig. 2 E&F). The average time between avalanches is 10 days, with a maximum of 29 days and a minimum of 2 h. Recurrence intervals were shorter in late March/early April, and in late April/early May (Fig. 4). Only one avalanche occurred in 56 days between 27 January and 24 March.

Approximate widths of the failed cornice section varied by a factor of 30 (Table 1). Linear modeling reveals that the width of the failed cornice has a significant positive correlation with the change in snow water equivalent (SWE) of the snowpack, temperature change, and mean SWE in the pre-avalanche interval (Table 2). Significant negative correlations were observed with the maximum rate of SWE decrease, the maximum rate of snow depth increase, cornice height, mean temperature, and mean snow depth (Table 2).

The heatmap produced by summing the avalanche debris fields reveals an area in the center of the field of view that is most affected by avalanche activity (Fig. 5). This area is located high in the snowbank beneath the cornice, but is offset slightly to the right from the location of the usual maximum cornice face height. Although less common, avalanches also affected areas in the extreme right and left sectors of the field of view. The lower limit of mapped avalanche debris reaches a common elevation across the toeslope of the snowbank.

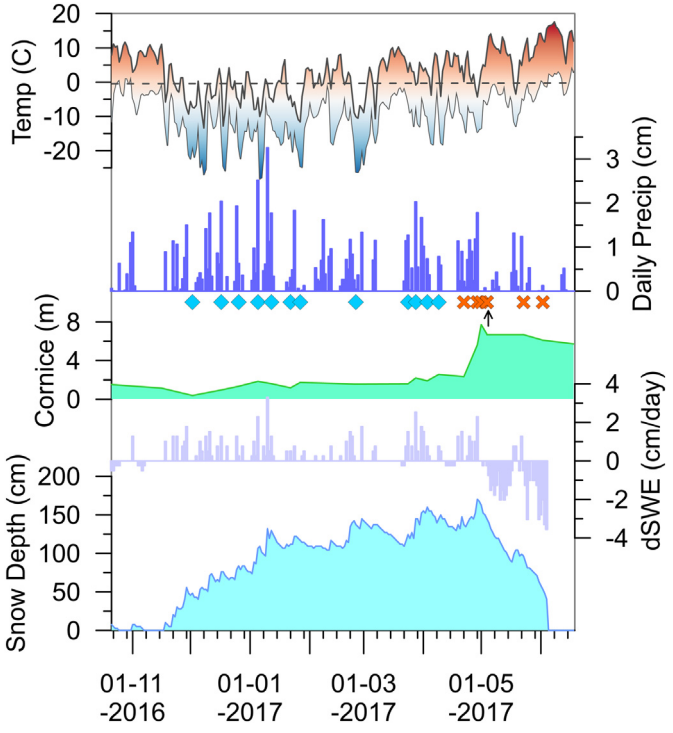

Fig. 4. Weather conditions during the camera deployment and recorded avalanche events. Snow depth was recorded at a SNOTEL station ~10 km north of the study site. dSWE is the daily change in snow water equivalent (SWE) of the snowpack. Height of the cornice face was estimated from the photographs using the measuring pole installed in the snowbank (Figs. 1D & 2A). Daily precipitation and temperature range are estimated for the snowbank site from the interpolated PRISM dataset. Blue diamonds represent individual avalanches inferred to have been caused by snow accumulation. Orange crossed represent avalanches inferred to have been caused by rapid temperature increases. The small arrow highlights Events 16 and 17, which occurred just 2 h apart and cannot be distinguished at this scale. (For interpretation of the references to color in this figure legend, the reader is referred to the web version of this article.)

3.3. Avalanche groups

Consideration of weather conditions in the pre-avalanche intervals supports assignment of the 19 recorded avalanches into two groups with contrasting causes. The first 12 avalanches appear to have been caused by snow loading on the cornice, both from snowfall and from wind redistribution. The photographs in which these avalanches were noted are preceded by intervals with significantly greater (P = 0.018) increases in snow depth, SWE, and precipitation (Fig. 6, Table 3), and these avalanches often occurred during times of temperature decrease. Wind speeds in the pre-avalanche interval averaged 8.6 m/s, in contrast to the mean of 7.8 m/s for the entire camera deployment. Linear modeling reveals a significant (or nearly significant) positive correlation between the width of the failed cornice in snow-caused events and both mean SWE and change in SWE (Table 2). A significant negative correlation was noted between failed cornice width and cornice height (Table 2).

In contrast, Events 13 through 19 appear to have been caused by rapid rises in temperature. Four of these events were preceded by temperature increases averaging 13.7 °C and mean rates of 2.0 °C/5 h (Table 3). Overall the difference between the temperature changes associated with snow- and temperature-caused avalanches is highly significant (P = 0.000, Fig. 6). Temperature-caused events were associated with significant (P = 0.041) decreases in SWE, implying rapid melting. Because they occurred later in the winter, temperatures were significantly (P = 0.003) warmer, mean SWE was greater (P = 0.007), and cornice faces (P = 0.000) were taller (Fig. 6, Table 3). Linear modeling demonstrates that the width of the failed cornice in these events is positively correlated with change in temperature and mean SWE (Table 2).

Snow water equivalent data and air temperature measurements from the SNOTEL site, and wind speed and direction from the Chepeta site, during each pre-avalanche interval are presented in Fig. 7. Major increases in SWE are clearly visible in the time associated with Events 1–5 and 7–12. A minor SWE increase occurred in the pre-avalanche interval for Event 6, which involved just a single, small block. In contrast, Events 13 and 15–19 were associated with major temperature increases and generally stable or falling SWE. Event 14 was a hybrid, where a major snowstorm was followed by a 12 °C temperature rise (maximum rate of 1.3 °C/5 h). However, given the dramatic temperature rise, Event 14 is assigned to the temperature-caused group.

4. Discussion

4.1. Advantages of time-lapse animation

A significant advantage of time-lapse photography from a fixed location is the ability to generate animations of landscape change that are visually compelling and intuitively interpretable. The animation produced in this project reveals several aspects of the annual cycle of this snowbank and cornice system that would not be readily apparent from individual photographs. For instance, two discrete areas of notably darker snow appeared in the snowbank during the last few weeks of ablation before the first major snowstorm of the winter (Fig. 2A). One, in the left sector, was visible shortly after the start of the camera deployment. The other, located in the lower center of the snowbank, appeared three weeks later. In the animation, both patches emerge and steadily enlarge until they are covered by the first snowstorm. With their darker appearance and strong visual contrast with the surrounding snow, these patches are likely firn representing snow from previous winters. The locations of these two patches generally correspond with the areas of greatest inferred snow depth (Fig. 1B), supporting the interpretation that they are composed of multi-year firn. In individual photographs or isolated field observations lacking the context provided by the time-lapse animation it would be simple to overlook these firn patches. However, their presence is an important indication of the interannual persistence of this snowbank, with ramifications for nivation processes (e.g. Matthes, 1900; Thorn, 1976).

The animation also provides the ability to monitor snow accumulation in response to the first storms of the season. Fig. 3 reveals that the 3.8-m tall measuring pole disappeared following three storms with notable snow accumulation accompanied by wind speeds in excess of 17 m/s. This observation is consistent with previous work concluding that windspeeds in excess of 10 m/s are necessary for cornice growth (Vogel et al., 2012). In the animation, the snowbank grows as waves of deeper snow prograde down the snowbank face. These layers thin with distance from the cornice. As a result, snow accumulation at a specific point, such as the measuring pole, is initially slow before increasing markedly. After the pole was buried, its known dimension on the original photographs can be used as a scale for snow depth later in the season, given the fixed perspective of the photographs. At the annual maximum in early May 2017, the animation reveals that the site of the measuring pole was covered by ~15 m of snow. Thus, time-lapse animations can add to our understanding of the conditions that foster cornice growth, and can provide the ability to estimate snow depth at specific study sites.

Finally, evidence of snow erosion is also captured in in the time-lapse animation. Significant scouring of the snowbank to produce a characteristic fluted surface (Allen, 1965) is visible at several points in the early winter. The appearance of this fluted surface was always preceded by high wind speeds. Winds in excess of 15 m/s in the absence of new snowfall scoured the snowbank surface on 1 November, and

Table 1
Recorded avalanches and climatic data.

Event	Trigger	Date	Interval*	Gap**	Width	Cornice	ΔSWE	SWE+	SWE-	mSWE	ΔDepth	Depth+	Depth-	mDepth	ΔPrecip	Precip+	ΔTemp	T+	T-	mT	mVel	mDir
#	–	–	Days	Days	pixels	m	cm	cm/5 h	cm/5 h	cm	cm	cm/5 h	cm/5 h	cm	cm	cm/5 h	°	°/5 h	°/5 h	°	m/s	°
1	Snow	2.12.16	–	2.1	436	0.4	0.8	0.1	0.1	7.4	5.1	0.5	−1.0	47.5	0.5	0.1	−9.8	1.6	−0.8	−11.6	4.3	334
2	Snow	17.12.16	15	1.9	84	1.0	1.8	0.3	−0.1	14.2	17.8	3.6	−1.0	74.2	1.8	0.3	−18.8	0.3	−1.8	−6.9	11.5	231
3	Snow	26.12.16	9	2.7	182	1.3	1.5	0.2	−0.1	16.3	20.3	3.0	−1.0	75.7	1.5	0.2	−14.3	0.2	−1.4	−8.2	12.8	184
4	Snow	05.01.17	10	2.0	76	1.9	2.8	0.2	−0.1	20.1	30.5	4.6	−2.5	95.8	2.8	0.3	−12.0	0.9	−1.1	−7.9	6.7	250
5	Snow	12.01.17	7	2.0	41	1.6	1.5	0.2	0.0	26.7	12.7	2.0	−0.5	125.0	1.5	0.2	−6.5	0.4	−0.5	−6.3	8.5	229
6	Snow	22.01.17	10	1.0	833	1.2	0.5	0.1	−0.1	28.4	7.6	1.0	−0.5	111.0	0.5	0.1	−10.0	0.6	−0.8	−10.6	8.6	307
7	Snow	27.01.17	5	3.0	1185	1.7	2.0	0.1	−0.1	29.5	15.2	1.5	−0.5	118.4	1.5	0.2	−15.3	0.9	−1.1	−12.0	7.7	300
8	Snow	25.02.17	29	2.7	380	1.6	1.0	0.2	−0.1	35.6	12.7	2.5	−1.0	140.5	1.3	0.2	−15.0	0.8	−1.3	−14.1	6.8	322
9	Snow	24.03.17	27	2.0	804	1.6	1.5	0.2	0.0	40.1	12.7	2.0	−1.5	119.6	1.8	0.2	8.0	2.4	−1.4	−1.2	8.6	222
10	Snow	28.03.17	4	1.0	578	2.2	2.0	0.3	0.0	44.2	20.3	3.0	−1.0	144.8	2.0	0.3	4.5	0.9	−0.5	−3.4	8.8	339
11	Snow	03.04.17	6	1.9	855	1.9	1.3	0.1	−0.1	48.3	10.2	1.0	−1.0	154.2	1.0	0.1	−11.5	2.3	−1.0	−3.5	7.7	331
12	Snow	09.04.17	6	1.0	346	2.6	1.0	0.1	0.0	49.8	12.7	1.5	−0.5	147.8	1.0	0.2	−9.0	0.9	−1.3	−6.9	10.8	252
13	Temp	22.04.17	13	1.0	1040	2.3	0.0	0.1	−0.1	51.6	−7.6	0.5	−1.0	136.9	0.0	0.1	18.0	−0.9	3.2	−2.5	6.1	328
14	Temp	29.04.17	7	2.1	462	5.6	2.5	0.3	−0.1	56.4	30.5	4.6	−2.5	165.1	2.3	0.3	12.0	1.3	−1.4	−6.7	9.1	341
15	Temp	01.05.17	2	1.9	527	7.7	0.0	0.1	−0.1	57.4	−15.2	0.0	−1.5	162.8	0.0	0.1	15.0	2.4	−0.8	−2.2	11.8	336
16	Temp	04.05.17	3	1.0	1069	6.7	0.0	0.2	−0.2	56.9	−7.6	0.5	−1.5	142.5	0.0	0.1	16.5	2.6	−1.8	5.7	4.8	339
17	Temp	04.05.17	0	0.1	382	6.7	0.0	0.0	−0.1	56.4	0.0	0.0	−0.5	137.2	0.0	0.1	−1.2	0.0	−0.9	10.6	1.1	265
18	Temp	23.05.17	19	17.0	487	6.7	−13.7	0.2	−0.4	44.2	−40.6	2.0	−1.5	103.9	3.3	0.2	−24.6	2.4	−2.0	2.8	8.3	235
19	Temp	02.06.17	10	0.9	62	6.1	−2.8	0.0	−0.5	24.1	−7.6	0.5	−1.5	52.6	0.0	0.1	11.4	1.8	−0.5	6.6	6.4	238

SWE-snow water equivalent.
Δ = maximum - minimun.
m-mean.
Vel-velocity.
* Time since previous avalanche.
** Time between before and after photographs.

Table 2
Results of linear modeling of failed cornice width for different avalanche groups.*

Avalanche group	Variable	Correlation type	Coefficient	P-Value	Interpretation: avalanches are larger with…
All	Change in SWE	+	701	0.000	greater snow accumulation
All	Change in Temperature	+	18	0.005	greater temperature rise
All	Mean SWE	+	36	0.014	more SWE in snowpack
All	Max rate of SWE decrease	−	−4220	0.000	minimal SWE decrease
All	Max rate of snowdepth increase	−	−380	0.001	slower rates of snow depth increase
All	Cornice height	−	−113	0.004	shorter cornice face
All	Mean Temperature	−	−41	0.006	lower temperatures
All	Mean snowdepth	−	−11	0.038	shallower snowpack
Snow-caused	Mean SWE	+	41	0.029	more SWE in snowpack
Snow-caused	Change in SWE	+	943	0.058	greater snow accumulation
Snow-caused	Cornice height	−	−943	0.050	shorter cornice face
Temperature-Caused	Change in Temperature	+	58	0.026	greater temperature rise
Temperature-Caused	Mean SWE	+	19	0.033	more SWE in snowpack

* Width of failed cornice is used as a proxy for avalanche magnitude. Linear modeling was conducted to identify variables contributing to larger avalanches. Analysis was first conducted for the set of 18 avalanches (excluding Event 18 for which the precursor conditions are poorly constrained). The analysis was then repeated using the subset of snow-caused (n = 12) and temperature-caused (n = 6) events. Only variables exhibiting P-values below ~0.05 are presented.

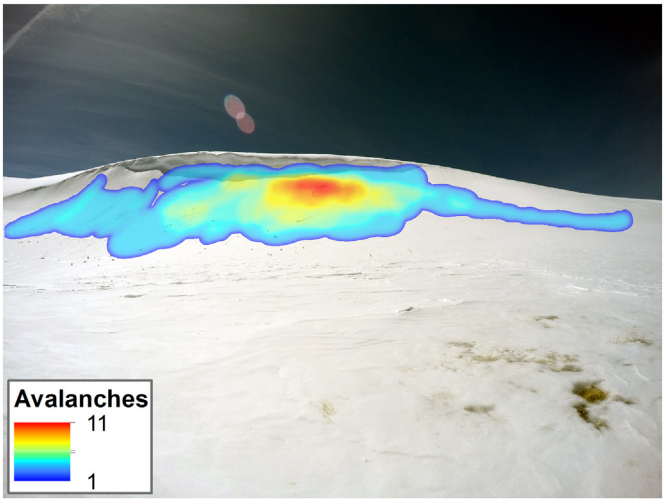

Fig. 5. Heatmap illustrating the relative frequency of avalanches across the face of the snowbank. Colors represent the number of avalanches in the winter of 2016–17 affecting a given part of the field of view; redder colors represent more frequent avalanches (maximum of 11 recorded events), and cooler colors represent less common avalanches (minimum of 1 event). Background photograph displays the snowbank on 3 May 2017.

again on 19 November, following the first major storm. Wind speeds in excess of 25 m/s caused extensive scouring in late November, before a snowstorm (26–29, November) delivered considerable snow leading to the first cornice collapse on 2 December (Fig. 3). The animation also reveals large snow ripples migrating at an oblique angle across the snowbank face in response to southerly winds following a snowstorm in late January. Combining time-lapse animation with meteorological monitoring, therefore, can illuminate conditions responsible for snow erosion and re-entrainment.

4.2. Avalanches and meteorological conditions

The 19 individual avalanches captured in the photographs fall into two distinct groups. The first 12 events are associated with significant increases in snow depth, SWE, and accumulated precipitation (Figs. 6& 7). As is shown in Fig. 4, these events accompanied many of the major snowstorms during the 2016–17 winter. Although there is some variability, winds during these storms were generally from the northwest with velocities > 7 m/s (Fig. 7, Table 1). These conditions would encourage rapid redistribution of snow across the surface of the plateau upwind from the snowbank (Fig. 1A), leading to rapid cornice growth (Meister, 1989; Vogel et al., 2012). This correspondence of avalanches with new snow and elevated windspeeds is consistent with previous work, which proposed snow loading as a major cause of cornice failure (Burrows and McClung, 2006; Schweizer et al., 2003). On the other hand, some observations of cornices suggest that although tension cracks form in response to storm-related loading events, actual failure happens weeks later, with a delay controlled by microtopography (Vogel et al., 2012). Because of the camera perspective in this study, it is not possible to determine whether the observed cornice failures happened along tension cracks that formed during previous storms.

The lull in avalanche activity observed during mid-winter further supports the connection between cornice collapse and snowfall. Only one avalanche was recorded between late January and late March. Fig. 4 reveals that very little snow accumulated during this interval and that the only avalanche, Event 8 on 25 February, happened in concert with the single notable increase in snow depth. This correspondence suggests that for approximately 2 months in the middle of winter the snowbank was stable with no major snow additions.

The last pulse of snow-caused avalanches occurred in late March and early April as snow depths approached their annual maximum. A series of storms 4–6 days apart delivered over 50 cm of snow with temperatures warmer than during storms earlier in the winter. Each storm was followed by cornice collapse events (Fig. 4, Table 1). Previous studies have noted that warmer temperatures weaken the snowpack by producing large temperature gradients in the upper layers (Eckerstorfer and Christiansen, 2011), and the role of snow loading in generating avalanche conditions is clear (Burrows and McClung, 2006; Schweizer et al., 2003). Most of these avalanches occurred in the same general sector of the snowbank, contributing to the avalanche hot spot clearly delineated in the heatmap (Fig. 5).

Avalanches in the second group, starting in late April, are associated with significantly warmer temperatures and greater temperature increases (Figs. 6&7, Table 1). Previous studies have noted increasing avalanche activity in late winter (Eckerstorfer and Christiansen, 2011) and concluded that that late season avalanches are driven by warmer temperatures (Burrows and McClung, 2006; Laute and Beylich, 2014). Warming of the upper snow layers would weaken the snowpack and increase rates of creep, leading to cornice failure (Eckerstorfer et al., 2013b; Eckerstorfer and Christiansen, 2011).

Temperature-caused avalanches are also associated with significantly greater snow depths (Fig. 6, Table 3), in part because of their occurrence in late winter when the snowpack reaches its annual maximum. In general, however, much of this snow accumulated during storms that were not directly associated with avalanches. For instance, 3 cm of SWE accumulated at the SNOTEL site between 19 and 21 April, but Event 13 occurred on 22 April when the temperature rose 18 °C

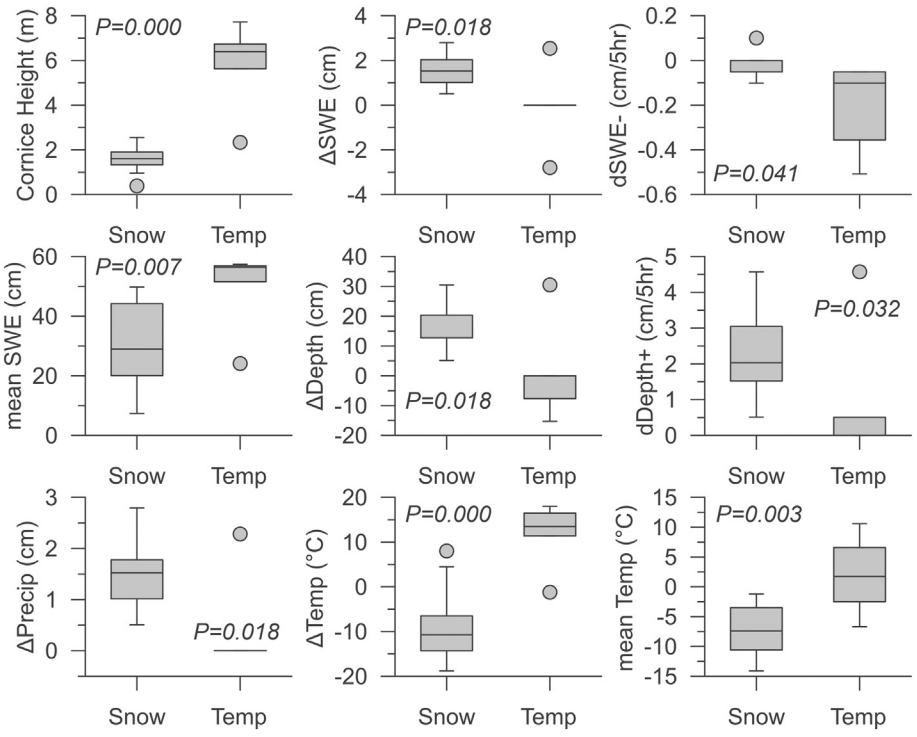

Fig. 6. Boxplots of metrics exhibiting significant differences in mean value between the snow-caused (Snow) and temperature-caused (Temp) avalanche groups. P-values are from a non-parametric Mann-Whitney test. Event 18 was not included in the significance calculations because its time of occurrence is imprecisely known due to a camera malfunction. Cornice height is estimated from the photographs given the measuring pole visible at the start of the deployment (Figs. 1D & 2A). SWE is snow water equivalent. Delta values are calculated for each pre-avalanche interval, defined as the period between the last photograph without avalanche evidence, and the first photograph with evidence of a new avalanche. Values of dSWE- and dDepth+ are the maximum rate of decrease (−) or increase (+), calculated as cm/5 h in each pre-avalanche interval. Weather conditions were recorded at a SNOTEL site ~10 km north of the study area.

Table 3
Comparison between snow- and temperature-caused avalanches.

Avalanche Cause						
Metric	Units	Snow	Temperature*	Mann Whitney U	Z-score	P
Interval	Days	11.6	5.8	19.5	−1.362	0.180
Gap	Days	1.9	1.2	16.0	−1.908	0.067
Area	pixels	100,793	123,393	24.0	−1.124	0.291
Width	pixels	483	590	29.0	−0.656	0.553
Cornice	m	1.6	5.9	1.0	−3.278	0.000
ΔSWE	cm	1.48	−0.04	11.0	−2.361	0.018
SWE+	cm/5 h	0.15	0.10	22.0	−1.341	0.213
SWE-	cm/5 h	−0.03	−0.16	14.5	−2.124	0.041
mSWE	cm	30.04	50.46	8.0	−2.624	0.007
ΔDepth	cm	14.82	−1.27	11.5	−2.313	0.018
Depth+	cm/5 h	2.20	1.02	13.0	−2.172	0.032
Depth-	cm/5 h	−1.01	−1.44	19.5	−1.601	0.125
mDepth	cm	112.9	132.8	22.0	−1.311	0.213
ΔPrecip	cm	1.44	0.38	11.0	−2.374	0.018
Precip+	cm/5 h	0.17	0.09	16.0	−1.946	0.067
ΔTemp	°	−9.14	11.95	2.0	−3.184	0.000
T+	°/5 h	1.02	1.20	30.0	−0.562	0.616
T-	°/5 h	−1.09	−0.38	31.0	−0.469	0.682
mT	°	−7.72	1.92	6.0	−2.811	0.003
mVel	m/s	8.6	6.6	23.0	−1.219	0.250
Azimuth	°	275	307	18.5	−1.640	0.102

* Excluding Event 18.

(Fig. 7). The snow accumulation may have contributed to instability of the cornice, but the dramatic temperature rise was likely the trigger. A major snowstorm occurred during the pre-avalanche interval for Event 14, but temperature rose dramatically late in the pre-avalanche interval after the storm ended (Fig. 7). No precipitation was associated with Events 15–17, and 19. More than 3 cm of precipitation accumulated in the 17 days preceding Event 18, however because the camera was dormant during this interval, the exact conditions associated with this avalanche cannot be determined. Although this event is plotted in Figs. 4 and 7 along with the other temperature-caused avalanches, it is not included in the Mann-Whitney analysis comparing the two avalanche groups (Fig. 6, Table 3).

It is also notable that temperature-caused avalanches are associated with significantly greater heights of the visible cornice face (Fig. 6). Heights remained consistently ~2 m for most of the winter, but jumped from 2.3 m to 5.6 m in late April at the same time that snow depths reached their maximum (Fig. 4). After this point SWE values remained steady and snow depths began to decrease. This correspondence suggests that the major jump in cornice face height was driven by a combination of factors. A major pulse of snow delivery coincided with relatively warmer temperatures, aiding sintering creep that increased the size of the cornice (Eckerstorfer et al., 2013b; Montagne et al., 1968). Simultaneously, collapse and avalanching of parts of the cornice may have increased the height of the face visible from the camera perspective.

The last two avalanches in late May and early June (Events 18 and 19) contrast with earlier events in both their location and (in the case of Event 19) their form. Both occurred far to the left across the face of the snowbank, contributing to the left-most extension of the avalanche heatmap (Fig. 5). Event 18 featured large blocks of snow that rolled down the snowbank surface below a clearly defined failure in part of the cornice that faces to the southeast, suggesting that direct solar heating was an important trigger. Solar radiation can impact snowpack stability similar to warming temperatures (Schweizer et al., 2003), and other studies using time-lapse cameras have noted an increase of avalanche activity controlled by direct solar radiation in late afternoon (Vogel et al., 2012) and in late winter (Laute and Beylich, 2014; Vogel et al., 2012). The last avalanche, Event 19, occurred farther to the left than any other event. Two distinct sections in the southeast facing sector of the cornice failed as flows that descended from point sources, widened 5-10× downslope, and terminated as rumpled sheets of snow and small blocks. The style of this movement resembles a wet loose snow avalanche, which have been shown to peak in late spring in response to meltwater production (Baggi and Schweizer, 2009).

4.3. Limitations and uncertainties

Although the experimental design employed in this project successfully captured visual evidence of cornice fall avalanches that could

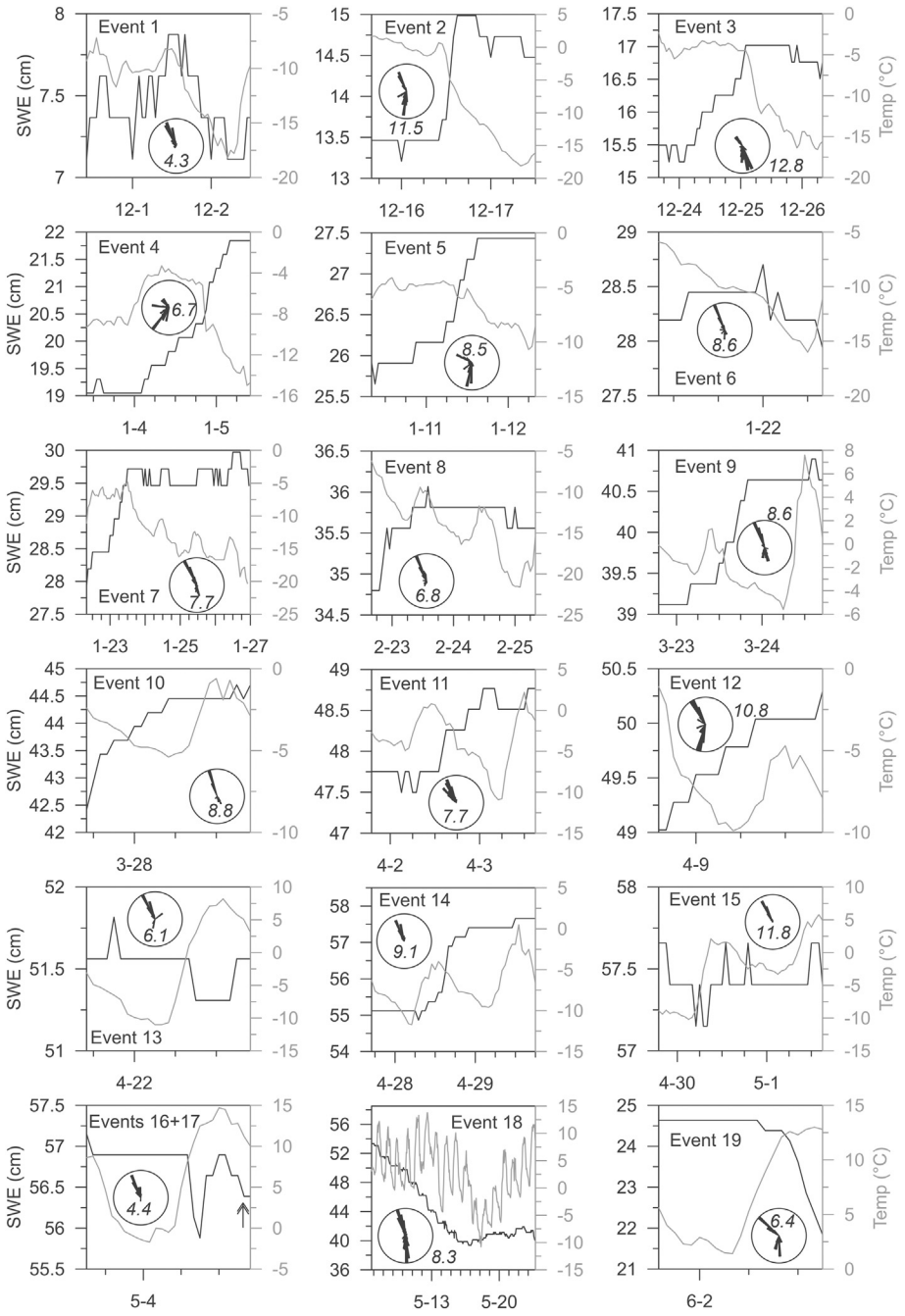

Fig. 7. Measurements of snow water equivalent (SWE) shown in black, and air temperature shown in gray, for each pre-avalanche interval at the SNOTEL station. Wind roses and mean wind speeds (in m/s) at the Chepeta weather station are also presented for these intervals. The pre-avalanche interval (x-axis) for each plot represents the time between the last photograph without evidence of an avalanche and the first photograph with clear evidence. Major ticks on x-axes are 1 day apart, except for Event 18 where major ticks are separated by 7 days. Events 17 occurred < 2 h after Event 16 (arrow). The camera was dormant for 2.5 weeks in May, so the timing of Event 18 is not well constrained. Events 1–12 are inferred to have been caused by additions of snow to the cornice. In contrast, Events 13–19 were likely caused by temperature increases.

be related to local meteorological variables, some inherent limitations constrain the scope of the resulting interpretations. One issue is that it cannot be determined whether an avalanche debris field visible in a given photograph was produced by a single event, or by a composite of multiple events. This uncertainty reflects the reality that avalanches occurring at night, during storms with decreased visibility, during intervals when the camera was dormant, or at frequencies higher than the temporal gap between consecutive photographs cannot be identified. Thus, the number of observed avalanches (19) is inherently a minimum value. On the other hand, the average gap between pre- and post-avalanche photographs is only 1.7 days (ignoring the interval preceding Event 18 when the camera was dormant). Thus, even if multiple avalanches were responsible for some debris fields, these likely occurred in response to the same meteorological conditions.

There are also inherent limitations related to the fact that temperature and precipitation data were recorded at a SNOTEL site ~500 m lower in elevation, and wind measurements were recorded at a weather station ~35 km away. While challenging, this situation is an unavoidable result of working in an area where the long-term installation of meteorological monitoring equipment is prohibited. Nonetheless, because this analysis focused more on temperature and precipitation trends rather than values, the uncertainty induced by this arrangement is considered acceptable. Furthermore, although the higher elevation snowbank location is colder and receives more snow than the SNOTEL site, interpolated data from the PRISM compilation indicate strong consistency in meteorological conditions between the two locations.

Less is known about how the wind speed and direction measurements at Chepeta relate to conditions at the snowbank study site. However, the elevations at the two locations are similar (Chepta 3860 m, Snowbank ~3840 m), as are the exposure and lack of trees. Furthermore, active wind transport of snow from the northwest is

visible on some photographs at times when the wind at the weather station was blowing from a northwesterly aspect. Thus, even if the wind velocities differed between the sites, the recorded aspects are likely similar.

Finally, the reality that this analysis focused on just a single snowbank constrains how widely the results can be extrapolated. Although the study site is not unique and resembles countless other snowbank and cornice systems in mountain environments, future work is necessary to determine how applicable the results reported here are to other sites.

5. Conclusion

Time-lapse photography was utilized to monitor evolution of a snowbank and associated cornice over an 8-month period. A 12-Mp digital camera, enclosed in a weatherproof case and supported by a 6-W solar array, was programmed to capture 5 photographs each day, centered on 12:00. Although battery issues during colder parts of the winter sometimes reduced the number of daily photographs, the camera captured nearly 700 useable images. These were combined to produce an animation documenting the extent and condition of the snowbank and cornice over an entire winter at a remote location that would otherwise remain unobservable. This animation reveals the presence of two cores of multi-year firn in the snowbank, illustrates the pattern through which the cornice and snowbank grow in response to early-winter storms, and records episodes of snow erosion through wind scouring.

The sequence of time-lapse photographs and related animation also document a total of 19 cornice fall avalanches, which is a minimum estimate for the number of events during the winter. Consideration of available meteorological data supports division of these avalanches into two categories with different causes. Twelve avalanches appear to have been caused by loading of snow onto the cornice. These were preceded by significant increases in snow depth, SWE, and precipitation, and windspeeds above the winter average. The size of these avalanches, as approximated by the width of the failed cornice, is related to both mean SWE and to the change in SWE.

In contrast, 6 of the last 7 avalanches appear to have been caused by rapid rises in temperature and increasing solar exposure. These were associated with decreases in SWE, warmer temperatures, greater mean SWE, and taller cornice faces. Linear modeling demonstrates that the width of the failed cornice in these events is positively correlated with change in temperature and mean SWE. The last avalanche, observed in early June, appears to have involved liquid water.

The results of this project underscore the strong potential of time-lapse photography as a tool for monitoring nival processes. The advantages of collecting hundreds or thousands of photographs of a study area over time, and combining these photographs as a time-lapse animation, greatly outweigh addressable concerns related to electronic sustainability and battery life (Eckerstorfer et al., 2016). As the costs associated with digital cameras and controllers continue to fall, more studies should consider this approach.

Acknowledgments

Thanks to T. Desautels, D. Munroe, and E. Norris for their help with the design and implementation of this project. The comments of two anonymous reviewers are appreciated.

References

Allen, J.R.L., 1965. Scour marks in snow. J. Sediment. Res. 35.
Baggi, S., Schweizer, J., 2009. Characteristics of wet-snow avalanche activity: 20 years of observations from a high alpine valley (Dischma, Switzerland). Nat. Hazards 50, 97–108.
Balog, J., 2012. Chasing Ice. National Geographic Documentary.
Burkhart, P.A., Alley, R.B., Thompson, L.G., Balog, J.D., Baldauf, P., Baker, G.S., 2017. Savor the cryosphere. GSA Today 27 (8), 4.
Burrows, R., McClung, D.M., 2006. Snow Cornice Development and Failure Monitoring, in: International Snow Science Workshop, Telluride Colorado.
Campbell, C.S., Egbert, S.L., 1990. Animated cartography/Thirty years of scratching the surface. Cartographica 27, 24–46.
Dohrenwend, J.C., 1984. Nivation landforms in the western Great Basin and their paleoclimatic significance. Quat. Res. 22, 275–288.
Dreier, L., Harvey, S., van Herwijnen, A., Mitterer, C., 2016. Relating meteorological parameters to glide-snow avalanche activity. Cold Reg. Sci. Technol. 128, 57–68.
Eckerstorfer, M., Christiansen, H.H., 2011. Topographical and meteorological control on snow avalanching in the Longyearbyen area, central Svalbard 2006–2009. Geomorphology 134, 186–196. http://dx.doi.org/10.1016/j.geomorph.2011.07.001.
Eckerstorfer, M., Christiansen, H.H., Rubensdotter, L., Vogel, S., 2013a. The geomorphological effect of cornice fall avalanches in the Longyeardalen valley, Svalbard. Cryosphere 7, 1361.
Eckerstorfer, M., Christiansen, H.H., Vogel, S., Rubensdotter, L., 2013b. Snow cornice dynamics as a control on plateau edge erosion in central Svalbard: Snow Cornice Dynamics Controlling Plateau Rim Erosion. Earth Surf. Process. Landf. 38, 466–476. http://dx.doi.org/10.1002/esp.3292.
Eckerstorfer, M., Bühler, Y., Frauenfelder, R., Malnes, E., 2016. Remote sensing of snow avalanches: Recent advances, potential, and limitations. Cold Reg. Sci. Technol. 121, 126–140.
Hendrikx, J., Peitzsch, E., Fagre, D., 2012. Time-lapse photography as an approach to understanding glide avalanche activity. In: Proceedings of the 2012 International Snow Science Workshop, pp. 872–877.
van Herwijnen, A., Fierz, C., 2014. Monitoring snow cornice development using timelapse photography. In: Proceedings of the International Snow Science Workshop, pp. 865–869.
van Herwijnen, A., Simenhois, R., 2012. Monitoring glide avalanches using time-lapse photography. In: International Snow Science Workshop ISSW, pp. 899e903.
van Herwijnen, A., Berthod, N., Simenhois, R., Mitterer, C., 2013. Using time-lapse photography in avalanche research. In: Proceedings ISSW, pp. 950–954.
Klett, M., 1984. Second View: The Rephotographic Survey Project. University of New Mexico Press.
Klett, M., 2004. Third views, second sights: a rephotographic survey of the American West. Museum of New Mexico.
Klett, M., Solnit, R., Wolfe, B., 2011. Repeat photography in landscape research. In: The Sage Handbook of Visual Research Methods, pp. 114–130.
Kobayashi, D., Ishikawa, N., Nishio, F., 1988. Formation process and direction distribution of snow cornices. Cold Reg. Sci. Technol. 15, 131–136.
Laute, K., Beylich, A.A., 2014. Morphometric and meteorological controls on recent snow avalanche distribution and activity at hillslopes in steep mountain valleys in western Norway. Geomorphology 218, 16–34. http://dx.doi.org/10.1016/j.geomorph.2013.06.006.
Malin, D., 2007. Time-lapse photography. In: The Focal Encyclopedia of Photography, Fourth Edition. Elsevier, pp. 622–623.
Matthes, F.E., 1900. Glacial sculpture of the Bighorn Mountains. Wyoming. In: US Geological Survey Twenty-first Annual Report Part II, pp. 167–190.
McCarty, D., Brown, R.L., Montagne, J., 1986. Cornices: their growth, properties, and control. In: International Snow Science Workshop, Lake Tahoe, pp. 41–45.
Meister, R., 1989. Influence of strong winds on snow distribution and avalanche activity. Ann. Glaciol. 13, 195–201.
Montagne, J., McPartland, J.T., Super, A.B., Townes, H.W., 1968. The nature and control of snow cornices on the Bridger Range, southwestern Montana. Montana State University.
Schweizer, J., Bruce Jamieson, J., Schneebeli, M., 2003. Snow avalanche formation. Rev. Geophys. 41.
Sturm, M., Holmgren, J., Liston, G.E., 1995. A seasonal snow cover classification system for local to global applications. J. Clim. 8, 1261–1283.
Thorn, C.E., 1976. Quantitative evaluation of nivation in the Colorado Front Range. Geol. Soc. Am. Bull. 87, 1169–1178.
Thorn, C.E., 1988. Nivation: a geomorphic chimera. Adv. Periglac. Geomorphol. 3–32.
Vogel, S., Eckerstorfer, M., Christiansen, H.H., 2012. Cornice dynamics and meteorological control at Gruvefjellet, Central Svalbard. Cryosphere 6, 157–171. http://dx.doi.org/10.5194/tc-6-157-2012.
Wahl, L., Planchon, O., David, P.-M., 2009. Characteristics and Seasonal evolution of firns and snow cornices in the High Vosges mountains (Eastern France). Erdkunde 63, 51–67. http://dx.doi.org/10.3112/erdkunde.2009.01.04.
Webb, R.H., 1996. Grand Canyon: A Century of Change: Rephotography of the 1889–1890 Stanton Expedition. University of Arizona Press.
Wilkinson, L., Friendly, M., 2009. The history of the cluster heat map. Am. Stat. 63, 179–184.